INSTITUTE OF PHYSICS PUBLISHING JOURNAL OF MICROMECHANICS AND MICROENGINEERING

J. Micromech. Microeng. **14** (2004) 1220–1229 PII: S0960-1317(04)76210-5

Optimization modeling of analyte adhesion over an inclined microcantilever-based biosensor

A-R A Khaled and K Vafai

Department of Mechanical Engineering, University of California, Riverside, CA 92521, USA

E-mail: vafai@engr.ucr.edu

Received 6 February 2004, in final form 30 April 2004
Published 17 June 2004
Online at stacks.iop.org/JMM/14/1220
doi:10.1088/0960-1317/14/8/015

Abstract

The effect of the microcantilever inclination on analyte adhesion is numerically analyzed in this work. A generalized model for the analyte adhesion is considered based on wall shear stress (WSS) at the microcantilever surface. Several analytical solutions for special cases are obtained. It is found numerically that the total mass transfer is enhanced by increasing the adhesion rate, the Peclet number and the use of converging flows over the microcantilever. Further, it is found that there exists a critical Peclet number that can maximize the total mass transfer when WSS slows down the adhesion process. The critical Peclet number increases as adhesion rate increases while it decreases as the flow becomes more convergent. Correlations are established on the basis of the numerical simulations for predicting flow operating conditions inside fluidic cells under maximized mass transfer rate conditions. Finally, this work paves the way for future experimental work in this area.

Nomenclature

A_p	projection of microcantilever area normal to the flow
a_p	area ratio
B	length of the interior channel
C	dimensionless concentration
C'	dimensional concentration
C_D	drag coefficient
C_m	mean bulk concentration
C_o	inlet concentration
D	mass diffusivity of the species
H	dimensionless height of the interior channel
h	dimensional height of the interior channel
h_o	inlet height of the interior channel
K	dimensionless adhesion rate
K_o	reference dimensionless adhesion rate
K_1	dimensionless adhesion rate constant due to wall shear stress
k	adhesion rate
k_o	reference adhesion rate
k_1	adhesion rate constant due to wall shear stress
Pe	Peclet number
p	fluid pressure
q_c	local mass transfer rate to the receptor coating
$(q_c)_t$	total mass transfer rate to the receptor coating
U	dimensionless axial velocity inside the interior channel
u	dimensional axial velocity inside the interior channel
u_i	average velocity inside the fluidic cell
u_m	average axial velocity inside the interior channel
u_{mo}	inlet average axial velocity inside the interior channel
V	dimensionless normal velocity inside the interior channel
v	dimensional normal velocity inside the interior channel
X	dimensionless axial coordinate
x	dimensional axial coordinate
Y	dimensionless normal coordinate
y	dimensional normal coordinate

Symbols

- Θ local dimensionless mass transfer rate to the receptor coating
- Θ_t total dimensionless mass transfer rate to the receptor coating
- ε perturbation parameter
- κ dimensionless slope of the microcantilever
- μ dynamic viscosity of the fluid
- ρ fluid density
- τ dimensionless time

1. Introduction

Advances in nanotechnology have revealed new prospects for biosensors. Examples of these biosensors are microsensors. These devices can be used to quickly detect, analyze and economically monitor chemical and biological agents in samples of a few microliters or less. As such, these devices possess a higher sensitivity relative to ordinary biosensors. Microsensors are pivotal in many applications. They are used to screen a patient for the presence of a disease or to determine its susceptibility to a given drug. Due to their high sensitivity, they become important for monitoring hazardous biological and chemical agents, toxins and chemical warfare agents.

A prominent engine driving the microsensor is the use of microcantilevers, which have been shown to be sensitive and accurate [1]. Microcantilever-based sensors have many important applications ranging from clinical analysis to environmental control and for monitoring hazardous biological and chemical agents, toxins and chemical warfare agents. This is because they quickly detect, measure, analyze and economically monitor chemical and biological agents in samples of a few microliters or less with no need for internal connections for power supply or other controlling devices. A microcantilever is commonly a bimaterial. The main substrate is made of silicon, silicon nitride, metal or combinations thereof. One side of the microcantilever is coated with gold so that a receptor coating can be deposited on this side. This receptor coating specifically binds to a given analyte (species being measured in an analytical procedure). Examples of receptor/analyte pairs are antibodies and antigens, complementary nucleotide sequences and receptors and small molecules [2].

Changes in the physical properties of a microcantilever after receptor/analyte bindings are used to detect changes in the surroundings. Most often the measured deflection of the microcantilever indicates the presence of a certain analyte [1–4]. When the analyte molecules bind to the receptor, the side coated with the receptor will either become tensioned or relieved, thereby causing the microcantilever to deflect. The concentration of the analyte is related to the deflection of the microcantilever. The magnitude of deflection is usually in nanometres. This deflection is usually measured using optical techniques. The performance of the microcantilever is affected by many factors. For example, Fritz *et al* [3] reported, in their experiment, that the deflection of the microcantilever due to flow disturbances and thermal effects could reach 5–10 times that due to analyte adhesion, respectively. This necessitates further analysis of the proper design of the fluidic cell and the microcantilever spacing within a biochip as discussed in [5–7].

Another important factor is related to the analyte adhesion rate at the receptor coating. Adhesion rates are found to be related to the wall shear stress (WSS) at the receptor surface. In certain applications, WSS at the receptor surface may enhance the adhesion rate as considered by David *et al* [8]. They used the shear stress to not only characterize the flow convective transport but also express the simple surface reaction mechanism used for modeling platelet adhesion at a wall surface. They found that if the wall reaction rate is chosen to be dependent on the WSS, then their analysis will be more realistic compared to the experimental evidence. In certain applications, the adhesion is found to decrease with WSS as shown in the work of Pritchard *et al* [9] who illustrated experimentally that high WSS prevents adhesion of monocytes to the vessel wall. Similar findings are illustrated in the works of Simon and Goldsmith [10] and Sapatnekar *et al* [11]. The data provided by Pritchard *et al* [9] suggest that the relation between the adhesion rate and the WSS can be approximated by a straight line. There have been many studies on the use of microcantilevers in sensing applications, but none addresses the optimization of analyte adhesion on the receptor coating by hydrodynamic considerations.

In this work, flow and mass transfer analysis are analyzed numerically over a microcantilever surface coated with a receptor. The microcantilever which is placed inside a microfluidic cell is allowed to be inclined with respect to the fluid flow. The adhesion rate at the receptor coating is linearly related to the WSS at the receptor coating. The governing equations are non-dimensionalized and solved numerically. The relationship between the total mass transfer rate at the receptor coating and the Peclet number, dimensionless slope of the microcantilever, height of the fluidic cell and the adhesion rate is established on the basis of the numerical simulation. In addition, the effect of flow disturbances and enhancements in the detection are analyzed and discussed.

2. Problem formulation

Consider a microcantilever placed inside a fluidic cell as shown in figure 1. The flow in the region occupied between the upper plate of the fluidic cell and the upper surface of the microcantilever is assumed to be two dimensional. This can represent the flow along the microcantilever centerline or for cases where the microcantilever width is relatively large. This region will be referred to as the interior channel. The length of the interior channel which is taken to be B and its height h are aligned along the x and y axes, respectively, as shown in figure 1. The microcantilever is considered to have an arbitrary inclination angle. The height h is related to the distance x according to the following relation:

$$h = h_o H = h_o \left(1 + \kappa \frac{x}{B}\right) \tag{1}$$

where h_o, H and κ are the height at the inlet of the interior channel, dimensionless height of the interior channel ($H = h/h_o$) and the dimensionless slope of the microcantilever, respectively.

The steady-state governing continuity, momentum and species mass balance equations are

$$\frac{\partial u}{\partial x} + \frac{\partial v}{\partial y} = 0 \tag{2}$$

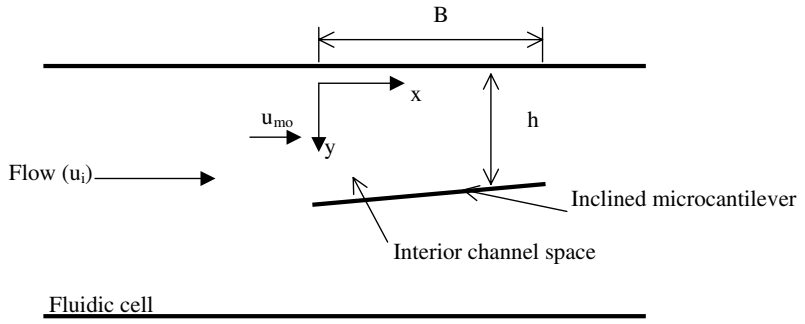

Figure 1. Schematic diagram and coordinate system.

$$\rho\left(u\frac{\partial u}{\partial x}+v\frac{\partial u}{\partial y}\right)=-\frac{\partial p}{\partial x}+\mu\left(\frac{\partial^2 u}{\partial x^2}+\frac{\partial^2 u}{\partial y^2}\right) \tag{3}$$

$$\rho\left(u\frac{\partial v}{\partial x}+v\frac{\partial v}{\partial y}\right)=-\frac{\partial p}{\partial y}+\mu\left(\frac{\partial^2 v}{\partial x^2}+\frac{\partial^2 v}{\partial y^2}\right) \tag{4}$$

$$u\frac{\partial C'}{\partial x}+v\frac{\partial C'}{\partial y}=D\left(\frac{\partial^2 C'}{\partial x^2}+\frac{\partial^2 C'}{\partial y^2}\right) \tag{5}$$

where u, v, p and C' are the axial velocity, normal velocity, pressure and the species concentration in the interior channel, respectively. The quantities D, μ and ρ are the mass diffusivity, absolute viscosity of the fluid and the fluid density, respectively. Most applications including microcantilever detection involve flows with small Reynolds numbers $\mathrm{Re} < 1$. This reveals that flow convective terms in equation (3), the terms on the right-hand side of equation (3), can be neglected. As such, the solution of the resulting equation yields the axial component of the velocity field while the normal component of the velocity field is obtained from the continuity equation, equation (2). The following are the resulting components of the velocity field:

$$u=6u_m\left[\left(\frac{y}{h}\right)-\left(\frac{y}{h}\right)^2\right] \tag{6}$$

$$v=\frac{6\kappa h_o u_m}{B}\left[\left(\frac{y}{h}\right)^2-\left(\frac{y}{h}\right)^3\right] \tag{7}$$

where u_m is the average velocity at each section ($u_m = u_{mo}h_o/h$; u_{mo} is the inlet average velocity for the interior channel). It is worth noting that when the microcantilever is inclined at significant angles, extra drag from the flow will be exerted on the microcantilever which may result in damage to the microcantilever head after long period of times.

In this work, steady-state conditions are assumed on the receptor coating which necessitates that available adhesion sites are constant over time. This type of analysis can be seen in many works including [8]. The adhesion at receptor coating can be modeled as follows:

$$D\frac{\partial C'(x,h)}{\partial n'}=kC'(x,h) \tag{8}$$

where k and n' are the adhesion rate and the distance measured in a direction normal to the microcantilever surface, respectively. The adhesion rate was found to be a function of the wall shear stress at the receptor coating surface [8]. The linear relation between the adhesion rate and the wall shear stress is considered in this work (see [8]). That is,

$$k=k_o-\mu k_1\left[\frac{\partial u(x,h)}{\partial y}+\frac{\partial v(x,h)}{\partial x}\right]. \tag{9}$$

2.1. Non-dimensionalizing of the governing equations

The following dimensionless variables are utilized:

$$X=\frac{x}{B} \tag{10a}$$

$$Y=\frac{y}{h_o} \tag{10b}$$

$$U=\frac{u}{u_{umo}} \tag{10c}$$

$$V=\frac{v}{(h_o u_{umo}/B)} \tag{10d}$$

$$C=\frac{C'-C'_o}{C'_o} \tag{10e}$$

where C'_o is a reference analyte concentration. Accordingly, equations (5)–(7) are represented as

$$U\frac{\partial C}{\partial X}+V\frac{\partial C}{\partial Y}=\frac{1}{Pe\varepsilon}\left(\varepsilon^2\frac{\partial^2 C}{\partial X^2}+\frac{\partial^2 C}{\partial Y^2}\right) \tag{11}$$

$$U=\frac{6}{H}\left[\left(\frac{Y}{H}\right)-\left(\frac{Y}{H}\right)^2\right] \tag{12}$$

$$V=\frac{6\kappa}{H}\left[\left(\frac{Y}{H}\right)^2-\left(\frac{Y}{H}\right)^3\right] \tag{13}$$

where Pe and ε are the Peclet number and the perturbation parameter for the interior channel, respectively. They are defined as

$$Pe=\frac{u_{mo}h_o}{D} \tag{14a}$$

$$\varepsilon=\frac{h_o}{B}. \tag{14b}$$

The dimensionless form of equation (8) is expressed as

$$D\frac{\partial C'(x,h)}{\partial n'}=DC'_o\left[\frac{(\varepsilon\kappa)}{\sqrt{1+(\varepsilon\kappa)^2}}\frac{1}{B}\frac{\partial C(X,H)}{\partial X}-\frac{1}{\sqrt{1+(\varepsilon\kappa)^2}}\frac{1}{h_o}\frac{\partial C(X,H)}{\partial Y}\right]=kC'_o(C+1) \tag{15a}$$

which further reduces to

$$\frac{1}{\sqrt{1+(\varepsilon\kappa)^2}}\left(\varepsilon^2\kappa\frac{\partial C(X,1)}{\partial X}-\frac{\partial C(X,1)}{\partial Y}\right)=K[C(X,1)+1] \tag{15b}$$

where $K = \frac{kh_o}{D}$. Equation (9) reduces to

$$k = k_o - \mu k_1 \left[\frac{\partial u(x,h)}{\partial y} + \frac{\partial v(x,h)}{\partial x} \right]$$
$$= k_o - \mu k_1 \left[\frac{u_{mo}}{h_o} \frac{\partial U(X,H)}{\partial Y} + \frac{\varepsilon u_{mo}}{B} \frac{\partial V(X,H)}{\partial X} \right]$$
$$= k_o - \frac{\mu k_1 u_{mo}}{h_o} \left[\frac{\partial U(X,H)}{\partial Y} + \varepsilon^2 \frac{\partial V(X,H)}{\partial X} \right]. \quad (16a)$$

Knowing that $\partial U(X,H)/\partial Y = -6H^2$ and $\partial V(X,H)/\partial X = 6\kappa^2/H^2$as can be shown from equations (12) and (13), equation 16(a) reduces to

$$K = K_o + 6\frac{K_1 Pe}{H^2}(1 - (\varepsilon\kappa)^2) \quad (16b)$$

where K, K_o and K_1 are defined as follows:

$$K = \frac{kh_o}{D} \quad (17a)$$

$$K_o = \frac{k_o h_o}{D} \quad (17b)$$

$$K_1 = \frac{\mu k_1}{h_o} \quad (17c)$$

and they will be referred to as the dimensionless adhesion or deposition rate at the receptor coating, the reference dimensionless adhesion or deposition rate and the dimensionless adhesion rate constant due to WSS effects, respectively.

2.2. Boundary conditions

The analyte concentration at the inlet of the interior channel is taken to be the reference concentration C'_o, while the concentration gradient at the upper boundary is considered to be zero. That is

$$C(0,Y) = 0 \quad (18a)$$

$$\frac{\partial C(X,0)}{\partial Y} = 0. \quad (18b)$$

The solution of equation (11) is almost independent of the concentration gradients at the exit of the interior channel since the Peclet numbers Pe for the pertinent applications tend to be greater than 500. In these cases, mass convection is much greater than the axial mass diffusion. Therefore, zero concentration gradients are imposed at the exit of the interior channel. It should be noted that non-slip conditions at the boundaries were implemented to deduce equations (6) and (7)

2.3. Calculated parameters

The main calculated parameters are the local dimensionless mass transfer rate Θ and the total dimensionless mass transfer rate Θ_t at the receptor coating surface. They are defined as follows:

$$\Theta(X) \equiv \frac{q_c h_o}{DC'_o} = K(C(X,H) + 1) \quad (19)$$

$$\Theta_t \equiv \frac{(q_c)_t h_o}{DC'_o B} = [K(C(X,H) + 1)]_{AVG}\sqrt{1 + (\varepsilon\kappa)^2} \quad (20)$$

where q_c and $(q_c)_t$ are the local mass transfer and total mass rates transferred to the receptor coating, respectively. As Θ_t increases, more analyte molecules are transferred to the receptor coating resulting in an enhanced detection capability of the microcantilever.

The scale analysis of equation (11) in the absence of axial diffusion effects and when $\kappa = 0.0$ suggests that the dimensionless mass transfer rate Θ near the inlet of the interior channel ($X < 0.1$; when $Pe = 500$ and $K_o = 20$) is equal to the following:

$$\Theta(X) \approx a \left\{ C(X,1) \left(\frac{6Pe\varepsilon}{X} \right)^{\frac{1}{3}} \right\}. \quad (21a)$$

The coefficient 'a' can be obtained by dividing the exact values of $\Theta(X)$ by the term in curly brackets in equation (21). This approximation is useful for interpreting how the local mass transfer is affected by different parameters such as Pe, ε and X.

2.4. Analytical solutions

For zero inclinations for the microcantilever ($\kappa = 0$), an analytical solution can be obtained for equation (11) using separation of variables when axial diffusion is neglected and when the velocity field is assumed to be uniform such that $U = 1$. For these conditions, equation (11) reduces to

$$Pe\varepsilon \frac{\partial C}{\partial X} = \frac{\partial^2 C}{\partial Y^2}. \quad (22)$$

The solution to equation (22) is

$$C(X,Y) = -1 + 4\sum_{n=1}^{\infty} \frac{\sin(\lambda_n)}{2\lambda_n + \sin(2\lambda_n)} \cos(\lambda_n Y)\, e^{-\frac{\lambda_n^2}{Pe\varepsilon}X} \quad (23)$$

$$\Theta(X) = 2K_o \sum_{n=1}^{\infty} \frac{\sin(2\lambda_n)}{2\lambda_n + \sin(2\lambda_n)} e^{-\frac{\lambda_n^2}{Pe\varepsilon}X} \quad (24)$$

where $\lambda_1, \lambda_2, \lambda_3, \ldots, \lambda_n, \ldots$ are the solutions of the following equation:

$$\tan(\lambda_n) = \frac{K_o}{\lambda_n}. \quad (25)$$

The total dimensionless mass transfer to the receptor coating is then

$$\Theta_t = 2K_o Pe\varepsilon \sum_{n=1}^{\infty} \frac{\sin(2\lambda_n)}{2\lambda_n^3 + \lambda_n^2 \sin(2\lambda_n)} \left(1 - e^{-\frac{\lambda_n^2}{Pe\varepsilon}} \right). \quad (26)$$

The obtained analytical solution can be used to approximate flow and mass transport inside a fluidic cell filled with certain pseudoplastic fluids (shear-thinning flow) such as flow of solutions and polymer melts.

2.5. Limiting case

When the binding affinity is relatively small or when the mass diffusivity of the species is relatively large, normal gradients can be neglected inside the interior of the channel. These cases belong to the condition where the dimensionless adhesion rate K is less than 0.1. For this condition, equation (11) can be

approximated by the following lumped model after integrating it over the interior channel height:

$$-K(C_{\mathrm{m}}(X)+1) = Pe\varepsilon \frac{\mathrm{d}C_{\mathrm{m}}(X)}{\mathrm{d}X} \tag{27}$$

where $C_{\mathrm{m}}(X)$ is the dimensionless mean bulk analyte concentration at each section in the interior channel. It is defined as

$$C_{\mathrm{m}}(X) = \int_0^H U(X,Y)C(X,Y)\,\mathrm{d}Y. \tag{28}$$

Solving equation (27) results in

$$C_{\mathrm{m}}(X) = \mathrm{e}^{-\frac{K}{Pe\varepsilon}X} - 1 \tag{29a}$$

$$\Theta_{\mathrm{t}}(X) = Pe\varepsilon\left(1 - \mathrm{e}^{-\frac{K}{Pe\varepsilon}X}\right). \tag{29b}$$

2.6. Flow disturbance effects on the microcantilever

The microcantilever is subjected to a drag force from the incoming flow. Part of this drag causes a permanent deflection to the microcantilever due to the mean flow while the other part may produce noise in the measurement due to the presence of the flow pulsations. The resulting drag force F_{D} on the microcantilever can be approximated by the following relation:

$$F_D \cong C_D \tfrac{1}{2}\rho(u_i)^2 A_{\mathrm{p}} \tag{30}$$

where C_{D}, u_{i} and A_{p} are the drag coefficient of the microcantilever, average velocity in the fluidic cell and the area of the microcantilever projected normal to the flow, respectively. Equation (30) represents an experimental correlation for the drag force. By definition, it accounts for the drag force on the body being equal to the total momentum force on the body when it is projected normal to the flow times a drag coefficient which is needed to be determined either theoretically or experimentally. This equation is widely used in different engineering applications involving flows over bodies with different shapes (e.g., [12]). The ratio of A_{p} to the microcantilever surface area is an important parameter for estimating how the microcantilever is affected by flow disturbances. This ratio is denoted by a_{p} and it is related to the interior channel configuration by the following relation:

$$a_{\mathrm{p}} = \sqrt{\frac{(\varepsilon\kappa)^2}{1+(\varepsilon\kappa)^2}}. \tag{31}$$

3. Numerical procedure

The more general equation for the mass balance of the species, which includes the transient effect of the concentration, has the following form:

$$\frac{\partial C}{\partial \tau} + U\frac{\partial C}{\partial X} + V\frac{\partial C}{\partial Y} = \frac{1}{Pe\varepsilon}\left(\varepsilon^2\frac{\partial^2 C}{\partial X^2} + \frac{\partial^2 C}{\partial Y^2}\right) \tag{32}$$

where τ is the dimensionless time. The first term on the left-hand side represents the transient effect of the species concentration. The solution of equation (32) for large times when steady-state conditions have been achieved collapses to the solution of equation (11). Equation (32) was transformed first to one with constant boundaries by using the following transformations: $\tau^* = \tau$, $\xi = X$ and $\eta = Y/H$.

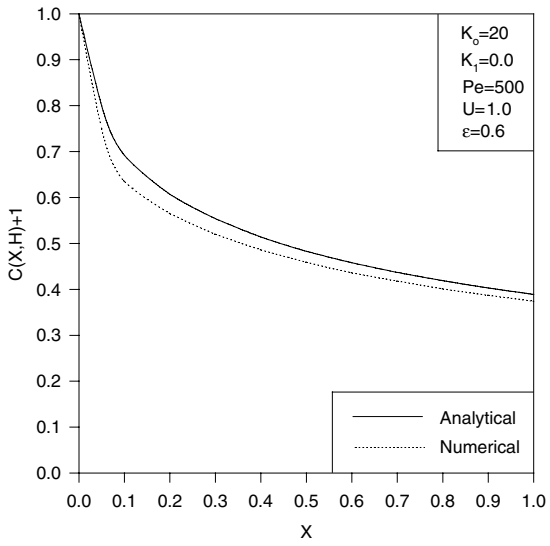

Figure 2. Comparison between analytical and numerical solutions.

Equation (32) was solved using an alternating direction implicit method (ADI) [13]. Central differencing in space was used for discretizing the dimensionless concentration differential terms while forward differencing was used to approximate the time differential term. Each time step is divided into two halves. In the first half, the X-gradients of the concentration are evaluated at the previous time step while Y-gradients of the concentration are discretized at the present half time step. The solution of equation (32) at the present half time step was then evaluated using a tri-diagonal algorithm [14]. For the next half time step, the solution at the previous half time step is utilized to obtain the Y-gradients of the concentration while X-gradients are discretized based on the concentrations at the present half time step. Accordingly, equation (32) was solved using the tri-diagonal algorithm and the procedure is repeated for each time step until steady-state conditions were achieved.

In this work, an arbitrary set of analyte and binding molecules are selected that have a strong binding affinity in order to investigate different phenomena that may be encountered. The reference values for the dimensional parameters were taken to be $u_{\mathrm{mo}} = 0.001$ m s^{-1}, $h_{\mathrm{o}} = 0.1$ mm, $D = 10^{-10}$ m^2 s^{-1}, $k_{\mathrm{o}} = 0.001$ cm s^{-1}, $k_1 = 5 \times 10^{-5}$ m^{-1} s^{-1}. This leads to the following reference dimensionless parameters: $Pe = 1000$, $K_{\mathrm{o}} = 10$ and $K_1 = 0.0005$ when the working fluid is water at 20 °C. The numerical solution of equation (11) was compared to the analytical solution presented by equation (24), when U is set to unity. Both solutions are plotted in figure 2 where good agreement is noticed between the results. A comprehensive study was also performed to determine the effects of the pertinent parameters on the mass transfer to the receptor coating. Moreover, the friction factor, a measure for the flow resistance, inside the fluidic cell in the absence of the microcantilever was validated against the experimental results of Park *et al* [15] which were conducted for microchannels. Figure 3 shows a comparison of the friction factor between the analytical solution of equation (3) in the absence of the convective terms and the experimental results of Park *et al* [15] for various Reynolds

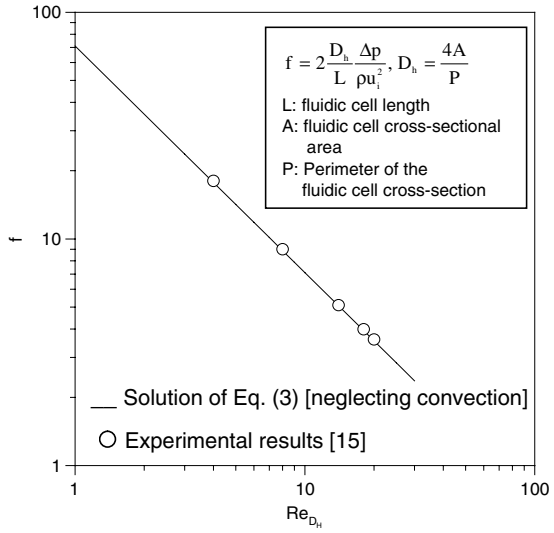

Figure 3. Comparison of the friction factor between the present study and that of Park *et al* [15] for various Reynolds numbers.

numbers. This figure illustrates that the obtained results are in excellent agreement with the experimental results. As such, the utilized continuum model represented by equations (6), (7) and (11) does provide a reliable estimation for the mass transfer rate over the microcantilever surface.

4. Discussion

4.1. Effects of the dimensionless reference adhesion rate K_o

Figure 4 illustrates the variations of the dimensionless local mass flux to the receptor coating as well as the depletion of the species mean bulk concentration in the interior channel for various dimensionless reference adhesion rates K_o. When adhesion rate increases, the resistance against species adhesion to the receptor coating decreases allowing for more species molecules to be deposited on the receptor surface (figure 4(a)). This in turn, causes a reduction in species concentration within the interior channel (figure 4(b)). The reduction in the mean bulk species concentration is relatively small since the Peclet number Pe is relatively large. Most of the mass transfer to the receptor coating is noted to be near the inlet of the interior channel (figure 4(a)). As such, allowing the fluid flow to travel over the microcantilever width direction is preferred over the case when the flow is along the direction of microcantilever length. The former case can enhance the adhesion of the species on the receptor coating. Ideally, increase in K_o enhances the adhesion rate on the microcantilever surface allowing most of the available adhesion sites on the receptor coating to be fully utilized by the analyte molecules in a shorter time period. As such, the detection by the microcantilever can be enhanced by an increase in K_o.

4.2. Effects of the interior channel height h

Figure 5 illustrates the effects of varying the interior channel height on the dimensionless total concentration at the microcantilever surface and the corresponding total mass transfer rate at $\kappa = 0$. The parameters Pe, K_o and ε increase linearly as h_o increases and Θ is also affected by an increase in h_o. As such, the parameter $\Theta(\varepsilon_o/\varepsilon)$ reflects the mass transfer rate at the microcantilever surface where ε_o is the perturbation parameter at a reference h_o value and ε is the effective perturbation parameter, $\varepsilon = h/B$. The parameters $(K_o)_o$ and $(Pe)_o$ represent the dimensionless adhesion rate and the Peclet number when the interior channel height is at the reference h_o value. As h increases, the velocity near the microcantilever surface decreases resulting in an inefficient mass convection near this region. As such, the concentration at the microcantilever surface decreases as h increases, as seen in figure 5(a). This, in turn, reduces the local mass transfer rate to the receptor coating as shown in figure 5(b). Therefore, thin fluidic cells are recommended to be used since the fluid flow will more closely adhere to the receptor surface resulting in an efficient mass convection. However, the associated increase in the wall shear stress on the microcantilever surface may reduce the effective residency time between the analyte molecules and the receptor (the expected time that the analyte mulecules are in contact with the receptor) which may reduce the adhesion rate as will be discussed later.

4.3. Correlation

Based on comprehensive set of numerical simulations, the following correlation is obtained for the total dimensionless mass transfer parameter Θ_t as functions of Pe, K_o and the dimensionless slope κ in the absence of the WSS effects on the adhesion rate.

$$\Theta_t = Pe^{0.177}(0.368 - 0.0611\kappa)K_o^{0.617} + \frac{1356}{PeK_o}. \qquad (33)$$

This correlation was established for the following range of parameters: $500 < Pe < 5000$, $-0.25 < \kappa < 0.25$, $5 < K_o < 20$ while K_1 was taken to be zero and $\varepsilon = 0.6$. The maximum difference between the correlation and the numerical results is less than 7%. According to correlation (33), maximum percentage increase in Θ_t is about 14% at the dimensionless inclination $\kappa = -0.25$. This expedites the detection of the microcantilever by a similar percentage and may enhance the microcantilever signal by increasing the number of utilized adhesion sites on the receptor coating within a fixed time interval. On the other hand, the ratio a_p increases from $a_p = 0$ at $\kappa = 0$ to $a_p \approx 0.14$ at $\kappa = -0.25$. That is, 14% of the microcantilever area is subject to normal drag forces due to either the mean flow or flow fluctuations. Note that both percentages are almost equal suggesting that the mean flow and flow fluctuations should be reduced in order to take advantage of the inclined microcantilever.

4.4. Effects of the adhesion rate constant due to WSS and the microcantilever slope

Figure 6 describes the effects of the adhesion rate constant due to WSS represented by K_1 and the microcantilever slope represented by κ on the dimensionless local mass transfer rate at the receptor as well as the dimensionless mean bulk concentration of the species. When WSS enhances the adhesion rate (positive K_1 values), convergent channels are good candidates to be used in order to enhance the adhesion rate as shown in figure 6(a). Thus, the microcantilever signal

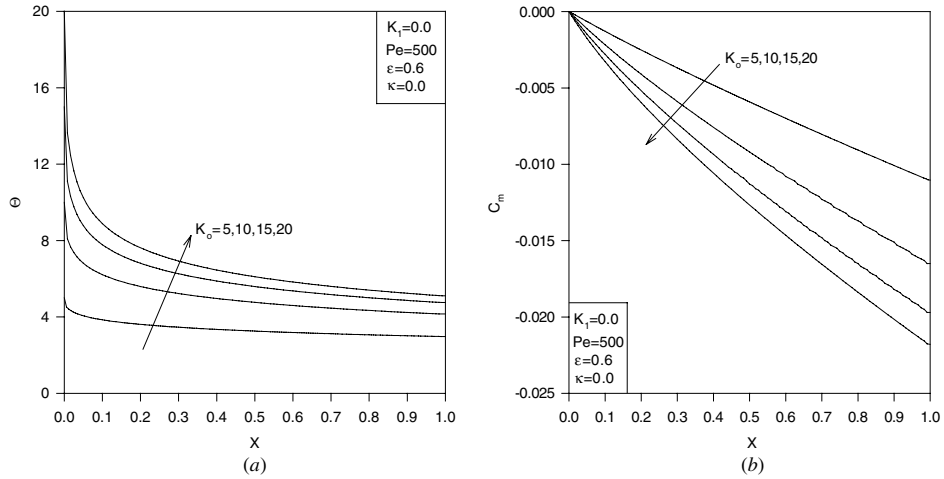

Figure 4. Effects of the dimensionless adhesion rate K_o on (*a*) dimensionless local mass transfer Θ and (*b*) mean bulk concentration C_m.

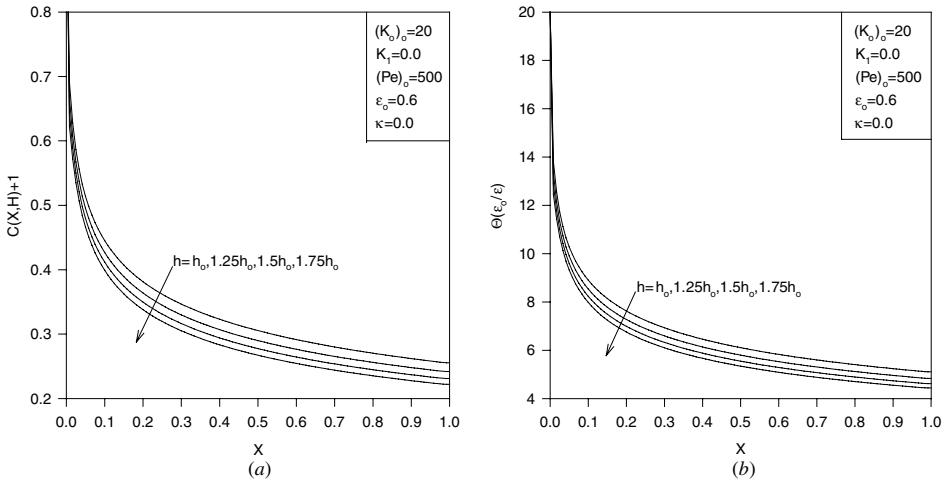

Figure 5. Effects of the interior channel height h on (*a*) the dimensionless concentration at the wall, $C(X, H)+1$ and (*b*) local mass transfer $\Theta(\varepsilon_o/\varepsilon)$.

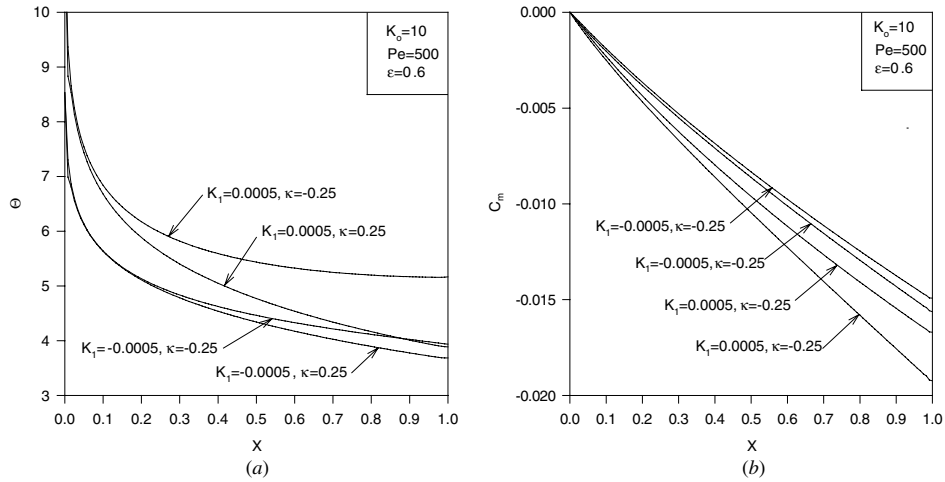

Figure 6. Effects of K_1 and κ on (*a*) dimensionless local mass transfer Θ and (*b*) mean bulk concentration C_m.

is enhanced by increasing the number of utilized adhesion sites on the receptor coating within a fixed time interval. In situations where WSS slows the adhesion process, divergent channels may expedite the adhesion process especially when the microcantilever slope is relatively large. In figure 6(*a*), the local mass transfer for $K_1 = -0.0005$ is found to be slightly greater when $\kappa = -0.25$ than when $\kappa = 0.25$. This indicates that divergent channels may be better than convergent channels

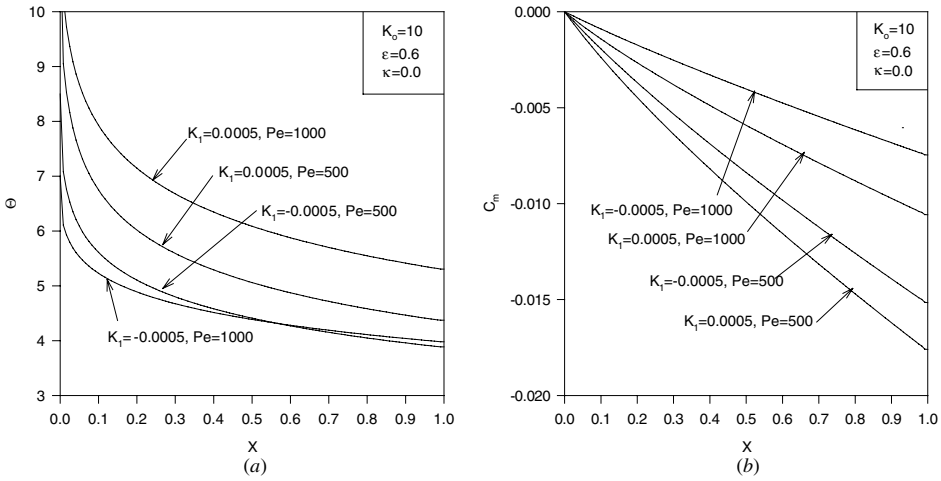

Figure 7. Effects of K_1 and the Peclet number Pe on (a) dimensionless local mass transfer Θ and (b) mean bulk concentration C_{m}.

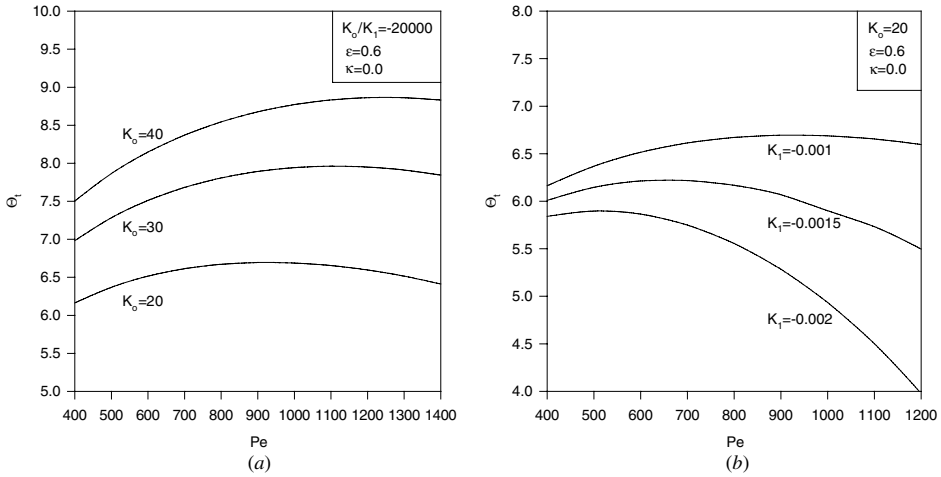

Figure 8. Variations of the dimensionless total mass transferred Θ_{t} with (a) K_{o} and the Peclet number Pe at a fixed value of K_1/K_{o} and (b) the Peclet number Pe and K_1.

for relatively large slopes. However, the area ratio a_{p} of the microcantilever is large for this range. As a result, the use of convergent channels is recommended except where WSS significantly slows down the adhesion process.

4.5. Effects of the adhesion rate constant due to WSS and the Peclet number

Figures 7(a) and (b) show the variation of Θ and the mean bulk concentration with X for different values of K_1 and Peclet number Pe, respectively. Although it is expected for the mass transfer rate to increase with an increase in Pe, figure 7(a) shows that the dimensionless mass transfer rate Θ is almost similar for both $Pe = 500$ and $Pe = 1000$ for this case where WSS slows down the adhesion process. As can be seen, Θ continues to increase as Pe increases when WSS enhances the adhesion process, as shown in figures 7(a) and (b). The enhancement in the mass transfer by an increase in Pe and the corresponding suppression in the adhesion due to WSS as Pe increases when K_1 is negative illustrates a new phenomenon. This phenomenon asserts that there is a critical Peclet number $(Pe)_{\mathrm{critcal}}$ for each analyte/receptor pair after which the mass transfer decreases with an increase in Pe. It is important to determine this critical Pe. Once $(Pe)_{\mathrm{critcal}}$ is determined, the operating conditions can be selected such that they will produce a Peclet number close to $(Pe)_{\mathrm{critcal}}$. This will result in full utilization of the receptor coating by maximizing the mass transfer rate to this coating.

4.6. Effects of the pertinent parameters on the critical Pe and the maximum mass transfer value

Figures 8(a) and (b) illustrate the effect of the Peclet number Pe, the dimensionless adhesion rate parameter K_{o} and the WSS parameter K_1 on the dimensionless total mass transfer Θ_{t} to the receptor coating. As K_{o} increases, the suppression in the adhesion process caused by WSS effects, when K_1 is negative, decreases. Thus, the critical Pe value increases as K_{o} increases, as shown in figure 8(a). Similarly, the maximum mass transferred to the receptor coating increases as K_{o} increases, as shown in figure 8(a). On the other hand, when K_1 decreases, the suppression in the adhesion process increases which results in a reduction in mass convection to the receptor coating. Since WSS effects on the adhesion process decrease as the dimensionless slope κ increases, the critical Peclet number $(Pe)_{\mathrm{critcal}}$ is expected to increase as κ increases

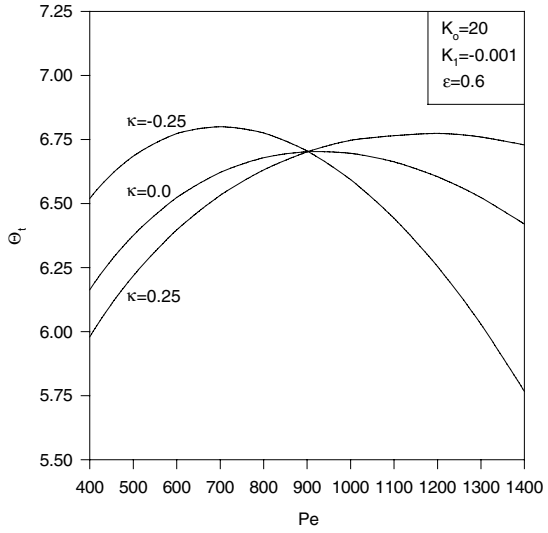

Figure 9. Variations of the dimensionless total mass transferred Θ_t with the Peclet number *Pe* and the dimensionless slope κ.

as seen in figure 9. However, the maximum mass transfer to the receptor coating is greater when the interior channel has a convergent configuration as seen in figure 9.

4.6.1. Correlations. The following correlations are obtained for the critical Peclet number $(Pe)_{\text{critical}}$, and the maximum total mass transfer rate parameter, $(\Theta_t)_{\max}$:

$$(Pe)_{\text{critical}} = (1.719\kappa^2 + 9.71\kappa + 9.467) \times (727\,680K_1^2 + 3240.96K_1 + 4.779)K_o^{1.265} \quad (34)$$

$$(\Theta_t)_{\max} = (0.21\kappa^2 - 0.0107\kappa + 0.979) \times (541\,80K_1^2 + 310.16K_1 + 1.399)K_o^{0.6}. \quad (35)$$

These correlations are valid for the following range of parameters: $-0.25 < \kappa < 0.25$, $20 < K_o < 40$ and $-0.001 < K_1 < -0.002$ while $\varepsilon = 0.6$. The maximum difference between the correlation and the numerical results is less than 6% of the numerical results for correlation (34) while it is less than 0.6% for correlation (35). According to correlation (35), the minimum total mass transfer rate to the receptor coating occurs at $\kappa = 0.025$ after which the mass transfer rate increases.

It is also noted that many values of the total mass transfer rate are repeated at two different microcantilever slopes as can be seen from equation (35). The first family of slopes produces convergent flows within the interior channel while the second one develops divergent flows inside the interior channel. Correlation (35) shows that the absolute value of the second family of slopes is greater than that for the first one. This leads to an increase in the microcantilever area facing the flow for the second family of the slopes. Accordingly, it is recommended to slightly incline the microcantilever such that a convergent flow is obtained over its active surface as the drag force for this case will be lower than the other family of slopes under a similar total mass transfer condition.

5. Conclusions

Optimization of analyte adhesion over an inclined microcantilever surface was analyzed numerically in this work. The adhesion rate at the microcantilever surface incorporated the dependence on the wall shear stress at the microcantilever surface. The governing equations were non-dimensionalized and solved on the basis of finite difference methods. Effects of a wide range of pertinent parameters such as Peclet number, adhesion constants, wall shear stress, microcantilever inclination and the height of the interior channel were thoroughly investigated. Analytical solutions were obtained for special cases.

It was found that converging flows along with thin fluidic cells enhance the mass transfer rate while decreasing the critical Peclet number that maximizes the mass transfer rate when the WSS slows down the adhesion process. The increase in the mass transfer rate at the microcantilever surface due to an increase in the Peclet number or for converging flows results in an enhancement in the microcantilever signal by increasing the number of utilized adhesion sites on the receptor coating within a fixed time interval. An increase in the Reynolds number or the use of convergent flows increases the flow disturbance effects on the microcantilever. Therefore, flow fluctuations should be minimized such that the resulting enhancement in the adhesion process is properly utilized while the noise level is minimized. Finally, the results in this work demonstrate the pathway for performing an experimental investigation in this area.

Acknowledgment

We acknowledge partial support of this work by DOD/DARPA/DMEA under grant number DMEA 90-02-2-0216.

References

[1] Wu G, Ji H, Hansen K, Thundat T, Datar R, Cote R, Hagan M F, Chakraborty A K and Majumdar A 2001 Origin of nanomechanical cantilever motion generated from biomolecular interactions *Proc. Natl. Acad. Sci. USA* **98** 1560–4

[2] Raiteri R, Nelles G, Butt H-J, Knoll W and Skladal P 1999 Sensing of biological substances based on the bending of the microfabricated cantilevers *Sensors Actuators* B **61** 213–7

[3] Fritz J, Baller M K, Lang H P, Rothuizen H, Vettiger P, Meyer E, Güntherodt H-J, Gerber Ch and Gimzewski J K 2000 Translating biomolecular recognition into nanomechanics *Science* **288** 316–8

[4] Yang M, Zhang X, Vafai K and Ozkan C S 2003 High sensitivity piezoresistive cantilever design and optimization for an analyte-receptor binding *J. Micromech. Microeng.* **13** 864–72

[5] Khaled A-R A, Vafai K, Yang M, Zhang X and Ozkan C S 2003 Analysis, control and augmentation of microcantilever deflections in bio-sensing systems *Sensors Actuators* B **94** 103–15

[6] Khaled A-R A and Vafai K 2004 Analysis of oscillatory flow disturbances and thermal characteristics inside fluidic cells due to fluid leakage and wall slip conditions *J. Biomech.* **37** 721–9

[7] Khanafer K, Khaled A-R A and Vafai K Spatial optimization of an array of aligned microcantilever-based sensors *J. Micromech. Microeng.* at press

[8] David T, Thomas S and Walker P G 2001 Platelet deposition in stagnation point: an analytical and computational simulation *Med. Eng. Phys.* **23** 299–312

[9] Pritchard W F, Davis P F, Derafshi Z, Polacek D C, Tsoa R, Dull R O, Jones S A and Giddens D P 1995 Effects of wall shear stress and fluid recirculation on the localization of circulating monocytes in a three dimensional flow model *J. Biomech.* **28** 1459–69

[10] Simon C and Goldsmith H 2002 Leukocyte adhesion dynamic in shear flow *Ann. Biomed. Eng.* 30 315–32

[11] Sapatnekar S, Kao W J and Anderson J M 1997 Leukocyte-biomaterial interactions in the presence of Staphylococcus epidermidis: flow cytometric evaluation of leukocyte activation *23rd Annual Meeting of the Society for Biomaterials (New Orleans, LA)* pp 409–20

[12] Yanaida K and Tanaka M 1997 Drag coefficient of a capsule inside a vertical angular pipe *Powder Technol.* **94** 239–43

[13] Hoffmann K A and Chiang S T 1998 Computational Fluid Dynamics: volume I 3rd edn Wichita, Kansas: Engineering Education System pp 337–52

[14] Blottner F G 1970 Finite-difference methods of solution of the boundary-layer equations *AIAA J.* **8** 193–205

[15] Park H, Pak J J, Son S Y, Lim G and Song I 2002 Fabrication of a microchannel integrated with inner sensors and the analysis of its laminar characteristics *Sensors Actuators* A **103** 317–29